Medical Devices and Diagnostic Engineering

Review Article ISSN: 2399-6854

Progress of nanotechnology for phototherapy: Fundamentals and applications

Jui-Teng Lin[1]*, Kuo-Ti Chen[2] and Hsia-Wei Liu[2,3]

[1]New Vision Inc. Taipei, Taiwan

[2]Graduate Institute of Applied Science and Engineering, Fu Jen Catholic University, New Taipei City, Taiwan

[3]Department of Life Science, Fu Jen Catholic University, New Taipei City, Taiwan

Abstract

We will review the recent progress of various nanoparticles for phototherapy with an emphasis on the fundamentals of synergic effects of photothermal therapy (PTT) and photodynamic therapy (PDT). Heat diffusion kinetics (to calculate the temperature increase of the heated nanoparticle), and photochemical kinetics for the efficacy of PDT, or the generation rate of reactive oxygen species are analyzed. The critical factors of the PTT/PDT synergic efficacy include: the absorption coefficients and concentrations of the nanoparticles and photosensitizers in the treated target, the exposure time, intensity and does (energy) of the light applied to the target. Efficacy of cancer therapy may be enhanced by combining PTT and PDT either activated by one light or two lights. For maximum synergic efficacy, the process order and the interaction between PTT and PDT are also important. To achieve the same efficacy, minimum dose and/or less exposure time for accelerated procedure by using a higher intensity (but same dose) are desired.

Introduction

Nanotechnology (nano-materials and nano-process) has been developed for both industrial and medical applications. The use of nano-medicine has been used in bio-imaging and bio-sensing, drug delivery, cancer cell diagnostics and therapeutics [1,2]. Nanoparticles (NPs) can cause tumor cell death by photothermal ablation, photodynamic toxicity, mechanical damage, or increase in the localized drug concentration. NPs are also promising agents for drug carriers, photothermal, photodynamic agents and contrast agents.

NPs used in biomedicine must meet some requirements such as non-toxic, chemically stable, biocompatible and uniform in size, shape and concentration. NPs are the excellent candidates for cancer therapy because of their targeting functions, sustained drug release profiles, reduced side effects, and the ability to overcome multidrug resistance. Various nanocomposites have been developed for modern medicine [1], including magnetite (Fe_3O_4), maghemite (γ-Fe_3O_4), cobalt iron oxide ($CoFe_2O_4$), titanium oxide (T_2O) and it alloys, silver, gold, mesoporous silica, cerium oxide (CeO2), stannum oxide (SnO_2), manganese oxide (MnO_2), praseodymium oxide (Pr_6O_{11}), antimony oxide (Sb_2O_3), zinc oxide (ZnO) and zirconium oxide (ZrO_2). In addition, mesoporous SiO_2 and carbon nanotubes (single- and multi-walled) have the potential to serve as a versatile drug nano-carrier for smart drug delivery because of their excellent properties such as high surface area and chemical stability.

Using surface plasmon resonance (SPR) in various shapes of gold nanoparticles (GNP), such as spheres, rods, boxes, cages and shells have been developed [3-10]. By changing the shape of GNP from spheres to nanorods, the absorption and scattering peaks change from visible to the near-infrared (NIR) regime. Comparing to the visible light, light in the NIR regime offers the advantages of larger absorption and scattering cross sections and much deeper penetration depth in tissues [5-7]. The red-shift of the absorption peak in gold nanorods is governed by the aspect ratio (defined by as the ratio of the length to the cross-sectional diameter), whereas it is governed by the shell thickness in nanoshells [5,6]. Lin et al., [8,9] proposed the use of a near IR diode laser system having multiple wavelengths for more efficient treatment of cancer tumor. To overcome the penetration issue, Lin et al., [8,9] also proposed the use of a train-pulse to increase the volume temperature increase which is particularly useful to larger volume tumors, unless an inserting fiber is used to deliver the laser energy. Various medical lasers and their fundamentals are reviewed by Lin [10].

NPs for dual-modality of fluorescence and magnetic resonance imaging-guided, and dual-therapy using photothermal therapy (PTT) and photodynamic therapy (PDT) have been developed recently [11-22], where synergic treatment modalities combining PDT with PTT could overcome current limitations of PDT, thus achieving enhanced anticancer efficacy.

GNPs are excellent tools for cancer cell imaging and basic research. However, the full potential for practical clinical outcomes requires the follow factors:

i. protection drugs from being degraded in the body before they reach their target;

ii. enhance the absorption of drugs into tumors and into the cancerous cells themselves;

iii. allows for better control over the timing and distribution of drugs to the tissue;

iv. prevent drugs from interacting with normal cells to limit side effects.

Correspondence to: Jui-Teng Lin, New Vision Inc. Taipei, Taiwan, E-mail: jtlin55@gmail.com

Key words: *nanotechnology, nanoparticles, photodynamic therapy, photothermal therapy, cancer therapy, photosensitizers, modeling*

Received: October 28, 2017; **Accepted:** November 27, 2017; **Published:** November 30, 2017

The animal study of Kim et al., [20] showed that tumor-targeting nanogel can function independently for both PDT and PTT and its synergy from the procedure of PDT followed by PTT, which is more effective than PTT followed by PDT. In addition to a review of clinical studies, we will propose modeling systems to analyze the synergic feature and explore the roles of key parameters influencing the anti-cancer efficacy.

The modeling systems

Phototherapy of cancers can be performed via: PTT, where the cancer cells are killed due to the temperature increase after light exposure; or PDT, where cancer cells are killed by singlet oxygen free radicals produced after a type-II process. As shown in Figure 1, the tumor cells killing efficiency may be enhanced by combining the photothermal therapy (PTT) and photodynamic therapy (PDT) using two light sources (either lasers or LED sources), in which the treated tumor tissue is injected by both nanogold solution and photosensitizers. Depending on the types of photosensitizers (PSs) and the shapes of the nanogold, the light wavelengths matching the absorption may vary from UV, visible to near IR (NIR). For examples, nanosphere absorbs visible light (at 480-680 nm), nanocube (700-900 nm), nanorod (700-2500 nm), and nanoshell (480-810 nm).

As shown in Figures 1 and 2, the combined PTT and PTT processes using various lights having wavelength from UV to IR with associate nanogold shapes and PS. Various PSs of riboflavin (B2), 5-ALA, methylene blue (MB) and indocyanine green absorb, respectively, light

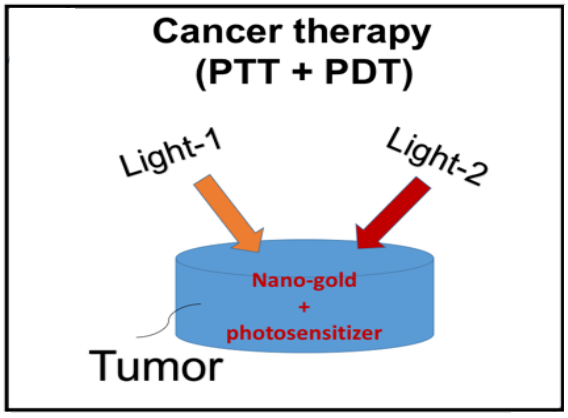

Figure 1. Combined PTT and PDT using 2 lights acting on the tumor nanogold injected with nanogold solution and photosensitizer [11].

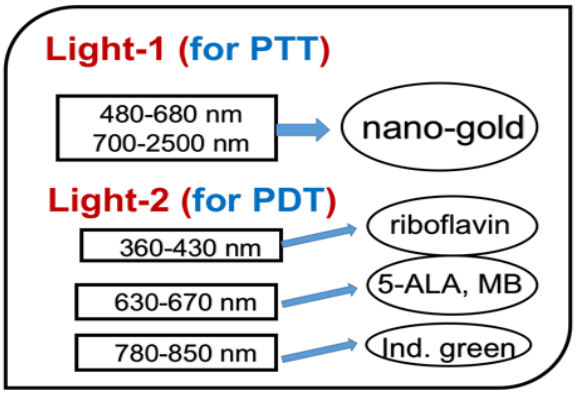

Figure 2. PTT/PDT processes using various UV and IR lasers with associate and photosensitizer [11].

at wavelength of (365, 430 nm), (530-670 nm), (780-850 nm), as shown by Figure 2. Therefore, a combined dual-function of PTT/PDT can be performed by: (a) an NIR light absorbed by both gold nanorod and indocyanine green; or a visible light absorbed by both gold nanosphere and 5-ALA; (b) two different lights having wavelength at NIR (for PTT) and UV to visible light (for PDT). For the case of one light for both PTT and PDT the simultaneously interacting with the nanogold and the photosensitizer is much more complex that of the case of two different lights which can be treated independently.

Figure 2 shows the dual therapy of PTT/PDT using two lights applying to various photosensitizers [11]. To analyze the efficacy of PTT and PDT, a heat diffusion kinetics will be used to calculate the temperature increase in PTT resulted from the nanogold absorption of light energy, whereas photochemical kinetics will be used to find the efficacy of PDT, or the generation rate of reactive oxygen species. The critical factors of the synergic therapy efficiency to be discussed include: the absorption coefficients and concentrations of the nanoparticles and photosensitizers in the treated target, the exposure time, intensity and does (energy) of the light applied to the target.

Analysis of photothermal therapy (PTT)

The temperature profile of the absorbing nano-medium after a laser (or LED) exposure may be governed by the following heat diffusion equation [8].

$$\frac{\partial^2 T}{\partial z^2} - \frac{1}{k}\frac{\partial T}{\partial t} - bT = -\left(\frac{AI}{K}\right)\exp(-Bz) \qquad (1.a)$$

where T is the temperature of the absorbing medium; z is the laser propagation direction along the depth of the medium, k and K are, respectively, the thermal conductivity and diffusivity of the solution; and b is the heat diffusion (per unit area) due to blood flow. I is the laser intensity (or power density), B is the extinction coefficient, which can be expressed by $B=[A(A+2s)]^{1/2}$, where s is the scattering coefficient; $A=\varepsilon C+Q$, ε is the absorption constant of the photosensitizer (PS), or nanoparticle, having an initial concentration C, and Q is the absorption constant of the tissue (without PS). In general, C(z,t) depends on both t and z, and can be depleted in PDT, especially in type-I process. If one includes this effect, coupled equations for dC/dt, and dI/dz are required and needed to be solved simultaneously with Eq. (1). In other words, the conventional Lambert-Beer law (BRL) for the light intensity needs to be revised to a time-dependent generalized LBL

$$I(z,t)= I0\ \exp[-A(z,t)] \qquad (1.b)$$

where

$$A(z,t) = 2.3\int_0^z [(\varepsilon_1 - \varepsilon_2)C(z,t) + \varepsilon_2 C_0 F(z) + Q]dz \qquad (1.c)$$

We note that A(z,t) is a decreasing function of time, when PS concentration, C(z,t), is depleted in time. The non-constant C(z,t) will affect both A and B in Eq. (1). Therefore, PTT is influenced by PDT if C(z,t) is not a constant. This interaction is small in Type-II process, or when Type-I is minor, then we may have solved for PTT independently to PDT. More details of above equation will be discussed later and defined in Eq. (2).

Eq. (1) requires numerical calculations. However, the steady-state solution can be obtained analytically, for the situation that C(z,t) of PS is not depleted, or A and B are Eq. (1) are constants [10]. Typical temperature increase ($dT=T-T_0$) profiles (temporal and spatial) are shown in Fig. 3 (A) and (B) for various laser intensity (10,20,30) mW/cm^2, with 500 sec exposure time. To kill cancer cells, typical temperature

needed are about 43 to 45°C, therefore a minimal of dT=6°C is needed, if T_0=37°C. As shown by Figure 3, higher intensity reaches a higher steady state temperature in about 15 to 30 minutes for A=3.0 (1/cm). As shown by Figure 3, volume temperature (z>0) is always lower than surface temperature in a cw operation. We have proposed a pulse-train method to increase the volume temperature [8] which is critical for tumors in large volume. In addition, multiple wavelength lasers (with different absorption coefficients and penetration depth) may be used for large size tumors. Concentration profile of the NPs inside the tumors is another parameter can be optimized to achieve maximum efficacy with minimum laser dose (energy). We have previously studied and analyzed in vitro photothermal destruction of cancer cells using gold nanorods and pulsed-train near-infrared [8,9]. However, the system was PTT only and the influence of concentration depletion or the interaction from PDT are not considered.

We should note that in vivo animal and/or human cancer therapy will be much more complex than in vitro under simplified conditions. These complexities shall include the non-uniform GNRs concentration in the tumor, the multi-layer normal-cancer tissue medium with multiple thermal parameters, and the blood flowing of the laser-targeted areas. This study with simplified conditions defined by uniform GNRs solution and controlled thermal parameters, however, still provides meaningful guidance based on vitro experimental measurements which are also consistent with theory. In addition, the design of multiple-wavelengths laser system shall partially overcome the issues of GNRs non-uniform and multiple thermal medium for a 3-dimensional-therapy, in which various absorption penetration depths are available via the fiber-coupled multiple-wavelength laser simultaneously targeting the cancer tumors.

A complete numerical simulation for the above complex system will be presented elsewhere. This study will emphasize on the efficacy of PDT.

Analysis of photodynamic therapy (PDT)

PDT makes use of PS to generate reactive radical species upon the absorption of specific wavelengths of light, where the selectivity is given by (i) PSs are preferentially taken up by tumour tissues, and (ii) the molecules generate cytotoxic radical species only at the site where light is administered. There are two cytotoxic photochemical mechanisms in PDT (as shown by Figure 4): (i) "Type-I" mechanism where the molecule directly reacts through its triplet excited state to generate reactive radical's species; and (ii) "Type -II" mechanism where PSs convert molecular oxygen into highly reactive singlet oxygen. Most PSs currently used in the clinic are predominantly "Type -II" molecules. It is also possible that both Type-I and -II coexist.

Depending on the target site, PDT effects can be divided into three different types: destruction of blood vessels, killing of tumour

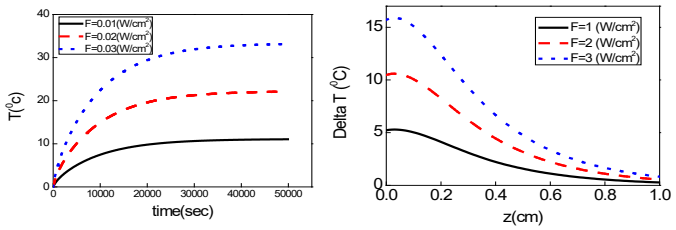

Figure 3. (A) Surface temperature increase profiles (at z=0) for various laser intensity (10,20,30) mW/cm². (B) Temperature increase spatial profiles for various laser intensity (10,20,30) mW/cm², with 500 sec exposure time.

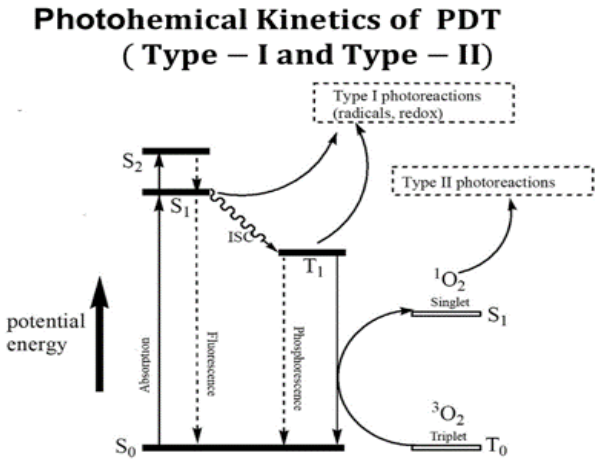

Figure 4. Photochemical kinetics of PDT (Jablonski diagram) showing type-I (with direct coupling to the target) and type-II mechanism (generating singlet oxygen) for anti-cancers. Additional reactive-oxygen-species (ROS) mediated type-I pathway may also contribute to the overall efficacy (not shown in the figure).

tissue and cells, and induction of immune response. If the PS is also mainly retained in the blood vessels, the type-II process produced singlet oxygen (SO) can damage the blood vessels, causing insufficient blood supply to the lesion, indirectly cause cell death. When the PS reaches the cell, SO may lead to cell apoptosis, necrosis and autophagy. The path of death depends on the concentration and distribution of SO in the course of treatment. In addition, many studies have shown that PDT for tumor cells itself has a strong immunogenicity, can stimulate the specific immune response. Its function to enhance tumor immunogenicity is also confirmed in the human body. Such as the use of photodynamic methods of laser local exposure to human basal cell tumor, there is no place to radiation, tumor cells also disappeared. This is because photo kinetics have improved the patient's active immune response to the tumor and will be automatically removed without irradiation, and have been validated in clinical trials of other tumor treatments.

PDT was theoretically studied by Forster et al., [21], Hu et al., [22], Wang et al., [23] and Zhu et al., [24, 25] for cancer therapy, and more recently by Lin [26,27] for corneal deceases which will be revised for cancer therapy in this study. Most photosensitizers (PS) available for PDT utilizes Type II photodynamic processes, i.e., the photodynamic effect is achieved through the production of singlet oxygen [21]. As shown in Figure 3 earlier and Figure 4, the process begins with the absorption of a photon by PS in its ground state, promoting it to an excited state. The PS molecule can return to its ground state by emission of a fluorescence photon, or convert to a triplet state, a process known as intersystem crossing (ISC). The triplet state may undergo a collisional energy transfer with ground state molecular oxygen (type II process), or with the substrate/target (type I process). In type II interaction, the PS returns to its ground state, and oxygen is promoted from its ground state (a triplet state) to its excited (singlet) state. In type-II process, the PS is almost not consumed (due to the slow singlet oxygen quenching rate), whereas in type-I process the PS is largely depleted specially for high intensity [26].

The life time of the singlet and triplet states of photosensitizer and the singlet oxygen are very short (ns to μs time scale) since they either decay or react with cellular targets immediately after they are created, therefore a set of quasi-steady state kinetic macroscopic kinetic equation for the concentration of the ground state PS, C(z,t), the ground state oxygen, $[O_2]$=X(z,t), and the light intensity, I(z,t) as follows [23,26,27],

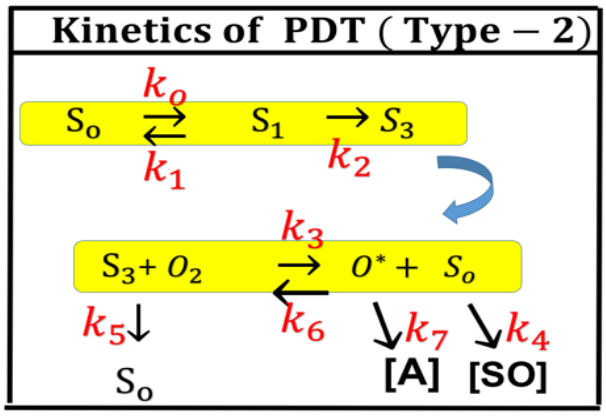

Figure 5. Photochemical kinetics of PDT in type-II process [27].

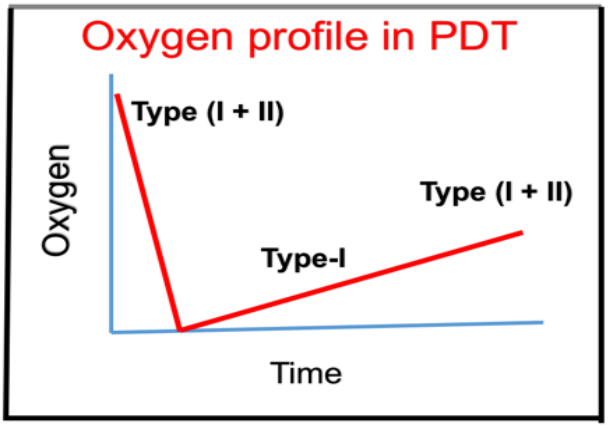

Figure 6. Typical oxygen profile in PDT, where oxygen is depleted in type-II and resupplied by diffusion, where type-I is dominant for low oxygen level [27].

$$\frac{\partial C(z,t)}{\partial t} = -aI(z,t)[fp + q\,G(z,t)]C(z,t) \quad (2.a)$$

$$\frac{\partial X}{\partial t} = -abI(z,t)G(z,t) + P(1 - \frac{X}{X0}) \quad (2.b)$$

$$\frac{\partial I(z,t)}{\partial z} = -A(z,t)I(z,t) \quad (2.c)$$

$$G(z,t) = C(z,t)X(z,t)/[X(z,t) + k] \quad (2.d)$$

$$A(z,t) = \varepsilon C(z,t)F(z) + \varepsilon' C_0 F(z) + Q \quad (2.e)$$

where $a=83.6\varepsilon\lambda/2.3$; λ is the light wavelength; ε and $\acute{\varepsilon}$ are the extinction coefficients of PS and the photolysis product, respectively; Q is the absorption coefficient of the normal tissue (without PS); p and q are the type-I and type-II quantum yield, respectively, given by $p= k_2/(k_1+k_2)$ and $q = pk_4/(k_6+k_7[A])$; $k= k_5/k_3$, $b= f'k_7[A]/ (k_6+k_7[A])$; and the type-I effective factor f= 1-g, with $g=[k_5+k_3X]/k_8[SH]$. P is the Oxygen diffusion and perfusion rate.

The effective factor (f) is 0 to 1.0 depending on the strength of the triplet PS direct coupling to the target (without via singlet oxygen). We note that type-I quantum yield (p) is also called as the "intersystem crossing rate" which defines the strength of the crosslinking [24].

Eq. (2) has been generalized for the situation that both type-I and type-II processes occur. It reduces to type-I only, when q=0, X(z,t)=P=0, or there is no oxygen supply in the process. The effective factor, defined by f= 1-g, with g being the effective regeneration of PS ground state due to type-II and type-I. that is the PS depletion in type-I is partially compensated by type-II. Reduction of the triplet PS molecule maybe due to its direct coupling to the target tissue [A] (in type-I), or its coupling to the singlet oxygen (in type-II). In general, type-I process occurs simultaneously with type-II, then type-II is terminated at the time oxygen is completely depleted. The effective regeneration factor (f=1-g) was ignored in previous modeling [21-25], which results an almost constant PS concentration, since qG (about 0.0001 to 0.001) is much smaller than f=1-g (about 0.1 to 1.0).

All the previous studies [21-25] assumed a type-II process (with p=0) and the PS is almost not consumed for the treatment period of 10 to 30 minutes, and therefore the light intensity is given by a time-independent Lambert-Beer law, that is C(z,t) in Eq. (2.e) is assumed to be a constant C_0. This is true only when type-II is dominated, and f<<q, type-I can be neglected. The initial concentration profiles (at t=0) of the PS and oxygen may be calculated or measured based on Fick's second law of diffusion. For analytic solution, we have chosen the distribution profile given by [26]: F(z,D) = 1-0.5z/D for PS solution, or C(z,t=0)=C0F(z), with a diffusion depth D in the stroma; and F'(D',z) =1-0.5z/D' for the oxygen initial concentration, or X(z,0)= X0F'(D',z), with a different diffusion depth D'. The typical diffusion depths are: D is 200 to 500 μm and D' is 100 to 200 μm.

The type-I efficacy Ceff (I)=1-exp(-S'), with S' function given by [26]

$$S'(z,t) = P(z,t)\sqrt{4fpK'C_0F(z)/(aI'(z))} \quad (3.a)$$

$$P(z,t) = 1 - \exp[-0.5atI'(z)] \quad (3.b)$$

where I'(z,t) = I0 exp(-A'z), with A' being an effective absorption constant. $K'=(k_p/k_t)^2$ with k_p and k_t are the rate constant for the polymer growth and termination; the effective factor, f=1 (or g=0), when type-II does not occur, or when the oxygen is completely depleted.

A complete numerical simulation will be shown elsewhere, and we will focus on analytic formulas to demonstrate the roles of each of the key parameters for type-II process, with type-I is ignored. The analytic formulas for the efficacy of type-II PDT as follows. Typical values of the parameters to be used in our calculations are (referred to Zhu et al., [24] for Photofrin as the sensitizer): P=0.015 (μM/s), p=0.8, q=0.001 (for [A]=830 μM), k=12.5, b=0.5 (with f'=0.5), Q=0.3(1/cm), ε=0.00036, or a=0.024 (for p=0.8), έ<< ε. Effective absorption constant A=3.5(1/cm), if includes the strong scattering constant of 14 (1/cm), or I(z)=I0 exp(-3.5z), when C(z,t) is almost constant. Initial values: C_0=8.5 μM, $[A]_0$=830 μM, $[^3O_2]_0$=83 μM. Solving Eq. (2.b), we obtain he oxygen concentration $[O_2]$ =X(z,t) is given by the following nonlinear equation (for P=0)

$$t= (83+4.43k-X-klnX)/B \quad (4)$$

with $B=0.085I_0\exp(-Az)$; and $t=t_0+X/P$, for P>0, t_0 defined by when X=0. Plotting the curve by changing X to obtain t (t *vs.* X) and rotated the coordinated by 90 degrees, we obtain the curve for X *vs.* t, which gives the oxygen profiles X(z,t). The time integration of X gives us the profile of singlet oxygen $[^1O_2]$, or $[O^*]$, and also the type-II efficacy defined by [24,27]

$$S = k_7[A]\int_0^t [Q^*]\,dt \quad (5)$$

Figures. 7-10 show the profiles of $[^3O_2]$, $[^1O_2]$, and S for various parameters (k,z,I,A,P), and their roles on anti-cancer are summarized as follows:

As shown by Figure 7, higher intensity depletes the oxygen faster than low intensity, and it starts from the surface (with higher oxygen for z>0).

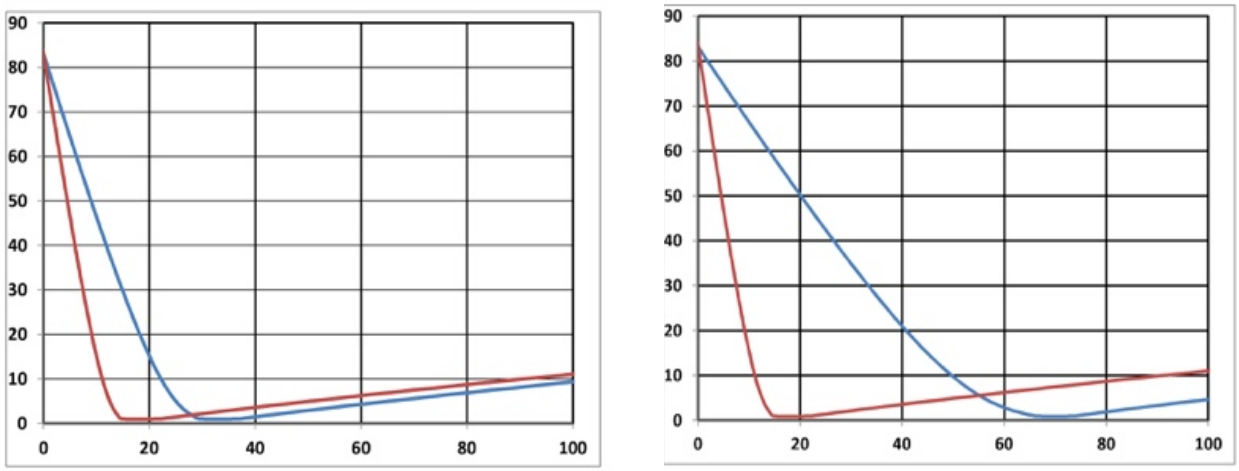

Figure 7. (A) Oxygen temporal profiles (A) on surface (z=0) for light intensity I_0 is 50 and 100 (red curve) mW/cm^2, k=10 (1/s), A=3.0 (1/cm), P=0.15 (1/s); initial value [O^2]=83 um, time in seconds. (B) for z=0 and 0.5 cm (green curve), and I=100 mW/cm^2.

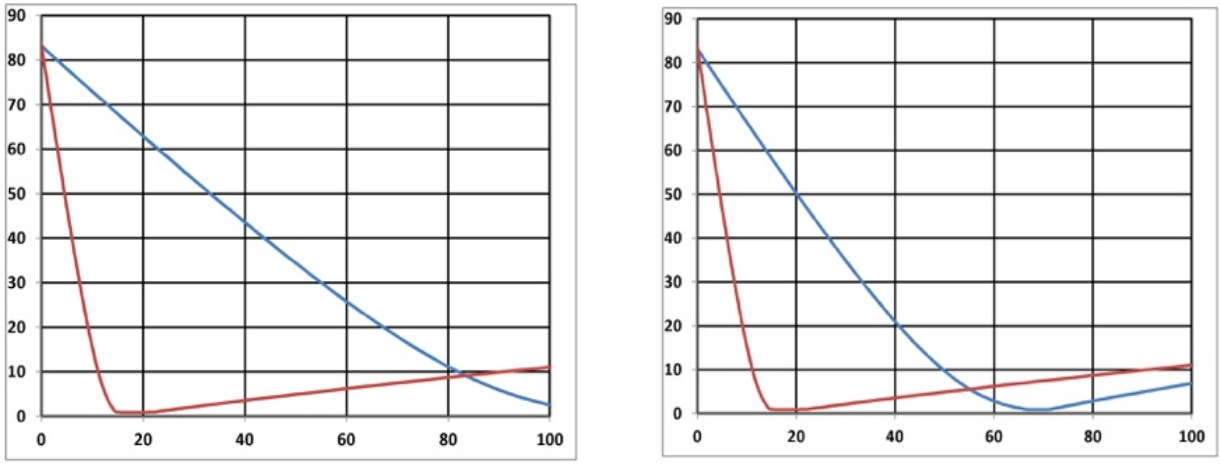

Figure 8. (A) Same as Fig. 9, but for z=0.5cm, A= 3.0 and 4.0 (1/cm) (green curve). (B) for A= 3.0 (1/cm), and P=0.15 and 0.23 (1/s) (green curve).

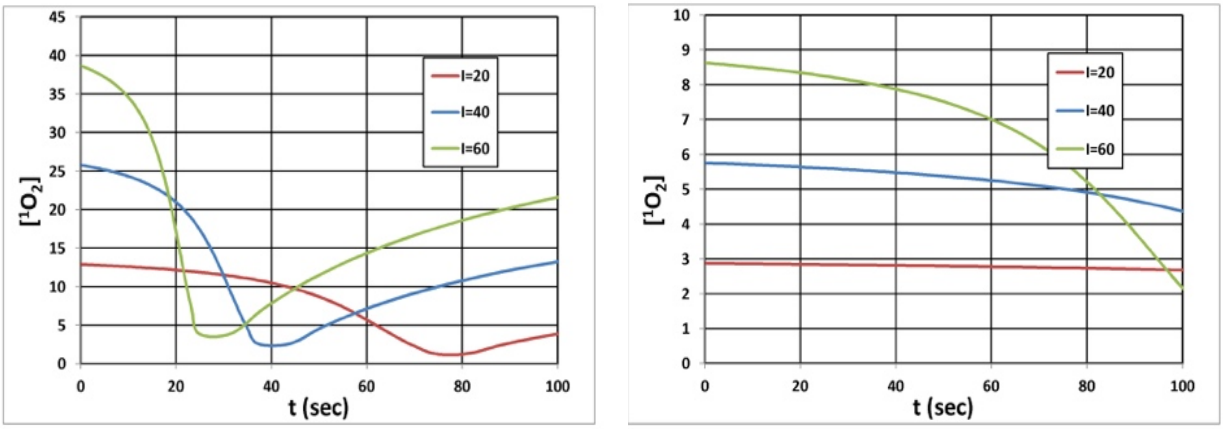

Figure 9. Singlet oxygen [$^1O_2$] temporal profiles: (A) on surface (z=0), and (B) at z=0.5 cm; for I_0= (20,40,60) mW/cm^2 curves in (red, blue, green). Other parameters are the same as Figure 8.

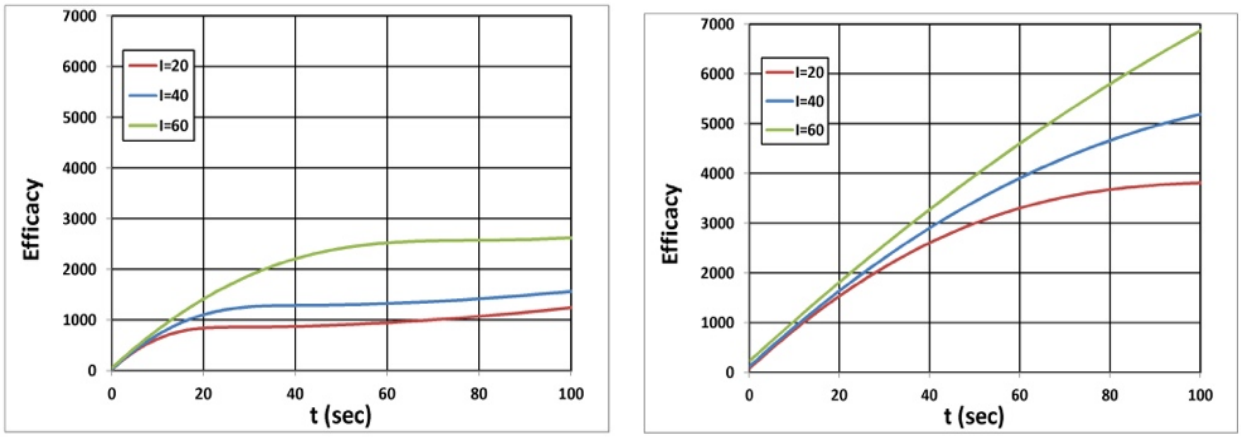

Figure 10. Efficacy profiles: (A) on surface (z=0), and (B) at z=0.5 cm, for I_0= (20,40,60) mW/cm^2 curves in (red, blue, green).

As shown by Figure. 8, higher absorption constant (A), or lower intensity (at a given depth) depletes the oxygen faster than low A.

As shown by Figure 9, higher oxygen diffusion rate (P) produces higher oxygen profiles.

As shown by Figure 10, higher intensity depletes the oxygen faster such that it produces higher singlet oxygen [$^1O_2$] and has higher efficacy.

Discussion of combined PTT and PDT

As shown in Figures 1 and 2, the tumor cells killing efficiency may be enhanced by combining PTT and PDT using two light sources (either lasers or LED sources), in which the treated tumor tissue is injected by both nanogold solution and photosensitizers. Depending on the types of photosensitizers and the shapes of the nanogold, the light wavelengths matching the absorption may vary from UV, visible to near IR (NIR). For examples, nanosphere absorbs visible light (at 480-680 nm), nanocube (700-900 nm), nanorod (700-2500 nm), and nanoshell (480-810 nm).

As shown in Figure 2, the combined PTT and PTT processes using various lights having wavelength from UV to IR with associate nanogold shapes and photosensitizer. Photosensitizer riboflavin (B2), 5-ALA, methylene blue (MB) and indocyanine green absorb, respectively, light at wavelength of (365, 430 nm), (530-670 nm), (780-850 nm), as shown by Figure 2. Therefore, a combined dual-function of PTT/PDT can be performed by: (a) an NIR light at NIR absorbed by gold nanorod and indocyanine green; or a visible light absorbed by gold nanosphere and 5-ALA; (b) two different lights having wavelength at NIR (for PTT) and UV to visible light (for PDT). For the case of one light for both PTT and PDT the simultaneously interacting with the nanogold and the photosensitizer is much more complex that of the case of two different lights which can be treated independently.

The animal study of Kim et al., [20] showed that tumor-targeting nanogel can function independently for both PDT and PTT and its synergy from the procedure of PDT followed by PTT, which is more effective than PTT followed by PDT due to certain interference from PTT, if it was applied to the system prior to PDT. As described earlier that A(z,t) and B(z,t) are decreasing function of time, when PS concentration, C(z,t), is depleted in time. The non-constant C(z,t) will affect both A and B in Eq. (1). Therefore, PTT is influenced by PDT, if C(z,t) is not a constant. This interaction is small in Type-II process, or when Type-I is minor, then we may have solved for PTT independently to PDT. The data shown by Kim et al., [20] implies that conducting PDT prior to PTT caused small or minimum depletion of C(z,t), such that it does not affect the A and B constant in Eq. (1) in solving the temperature increase. However, we believe that Type-I and -II processes most likely to co-occur, and certain degree of PS concentration is depleted after the PDT. This influence is more significant when z>10 mm, or when the amount of A(z,t) decrease affecting more on the light intensity I(z,t) when calculating the temperature. Smaller A or B in Eq. (1) will achieve deeper light penetration, but also shows an optimal related by $A^*z=1.0$, or $A^*=1/z$, and smaller A^* achieves deeper z. When two lights are used independently for PTT and PDT, the system modeling is simpler than when only one light is used for PTT/PDT, in which Eq. (1) and (2) must be solved simultaneously.

Optimal synergetic efficacy of PTT/PDT depends on not only the order of PTT and PDT but also how the light (or lights) is applied. Parameters involved in the optimal process shall include at least the dynamic of time-dependent PS concentration, C(z,t) , and light intensity I(z,t), the optimal penetration depth (for both PTT and PDT), the total dose (or energy), and the associate light intensity and exposure time. Efficacy should be also optimized by a minimum dose and/or less exposure time, where procedure maybe accelerated by using a higher intensity (but the same dose), which has been demonstrated in different application of PDT called corneal crosslinking deceases [26,27]. A complete numerical simulation will be shown elsewhere.

In addition to the PTT/PDT synergistic method presented earlier, the efficacy of PDT may be further improved significantly via conjugated nanogolds. For example, it was reported by the conjugated spherical nanogold as the delivery agent for 5-ALA resulted in a two times higher cell death rate compared to free 5-ALA [28]. Another example is that the DNA damage caused by PDT as demonstrated by alkaline gel electrophoresis was greater in the methylene blue (MB) plus chitosan-treated group than in control and MB-treated groups [29]. As indicated earlier, using near IR light in PDT is required for large size tumours. Therefore, the available IR-light response PSs are important. An updated overview on the development of new photosensitizers for anticancer photodynamic therapy was reported by Zhang et al., [30]. More clinical studies of the efficacy of PDT and PTT using various nanoparticles have been reported [31-39].

Conclusion

Efficacy of cancer therapy may be enhanced by combining PTT and PDT either activated by one light or two lights. For maximum PTT/PDT synergistic efficacy, the concentration of PS and nanoparticles

required to be optimized in addition to the wavelength of the light matching the absorption peak of PS and nanoparticles. To achieve the same efficacy, minimum dose and/or less exposure time for accelerated procedure by using a higher intensity (but same dose) is highly needed.

References

1. Bhuiyan MTH, Chowdhury MN, Parvin MS (2016) Potential nanomaterials and their applications in modern medicine: an overview. *ARC Journal of Cancer Science* 2: 25-33.
2. Shafirstein, G. Battoo A, Harris K, Baumann H, Gollnick SO, et al. (2016) Photodynamic therapy of non-small Cell Lung Cancer. Narrative Review and Future Directions. *Ann Am Thorac* Soc 13: 265-275. [Crossref]
3. Huang X, El-Sayed MA (2010) Gold nanoparticles: Optical properties and implementations in cancer diagnosis and photothermal therapy. *J Advanced Research* 1: 13-28.
4. Popp MK, Oubou I, Shepherd C, Nager Z, Anderson C, et al. (2014) Photothermal therapy using gold nanorods and near-infrared light in a murine melanoma model increases survival and decreases tumor. *J Nanomaterials* 2014.
5. Lin JT (2011) Nonlinear optical theory and figure of merit of surface plasmon resonance of gold nanorods. *J Nanophotonics* 5: 051506.
6. Lin JT (2010) Scaling law and figure of merit of biosensor using gold nanoshells. *J Nanophotonics* 4: 049507.
7. Lin JT (2013) A generalized geometric factor for unified scaling law for bio-sensor based on nanostructures of gold. *Inter J Latest Res Science and Tech* 2: 23-25.
8. Lin JT, Hong YL, Chang C (2010) Selective cancer therapy via IR-laser-excited gold nanorods. *SPIE BiOS* 7562: 75620R.
9. Lin JT, Chiang S, Lin GH, Lee H, Liu HW, et al. (2012) In vitro photothermal destruction of cancer cells using gold nanorods and pulsed-train near-infrared lase. *J Nanomaterials* 2012.
10. Lin JT (2016) Progress of medical lasers: Fundamentals and Applications. *Medical Device Diagn Eng* 1: 36-41.
11. Lin JT (2016) Analysis of the efficiency of photothermal and photodynamic cancer therapy via nanogolds and photosensitizers. *J Cancer Research Update* 6: 12-18.
12. Wang YH, Chen SP, Liao AH, Yang YC, Lee CR, et al. (2014) Synergic delivery of gold nanorods using multifunctional microsbubbles for enhanced plasmonic photothermal therapy. *Scientific Report* 4: 5685. [Crossref]
13. Zhang H, Li YH, Chen Y, Wang MM, Wang XS, et al, (2017) Fluorescence and magnetic resonance dual-modality imaging-guided photothermal and photodynamic dual-therapy with magnetic porphyrin-metal organic framework Nanocomposites. *Scientific Reports* 7: 44153.
14. Shirata C, Kaneko J, Inagaki Y, Kokudo T, Sato M, et al. (2017) Near-infrared photothermal/photodynamic therapy with indocyanine green induces apoptosis of hepatocellular carcinoma cells through oxidative stress. *Scientific Reports* 7.
15. Wang P, Tang H, Zhang P (2016) Plasmonic nanoparticle-based hybrid photosensitizers with broadened excitation profile for photodynamic therapy of cancer cells. *Scientific Reports* 6: 34981.
16. Lv R, Wang D, Xiao L, Chen G, Xia J, et al. (2017) Stable ICG-loaded upconversion nanoparticles: silica core/shell theranostic nanoplatform for dual-modal upconversion and photoacoustic imaging together with photothermal therapy. *Scientific Reports* 7: 15753.
17. Wang S, Huang P, Nie L, Xing R, Liu D, et al. (2013) Single continuous wave laser induced photodynamic/plasmonic photothermal therapy using photosensitizer-functionalized gold nanostars. *Adv Mater* 25: 3055-3061. [Crossref]
18. Khlebtsov B, Panfilova E, Khanadeev V, Bibikova O, Terentyuk G, et al. (2011) Nanocomposites containing silica-coaged gold–silver nanocages and multifunctional capability of IR-luminescence detection, photosensitization, and photothermolysis. *ACS Nano* 5: 7077-7089.
19. Tian B, Wang C, Zhang S, Feng L, Liu Z, et al. (2011) Photothermally enhanced photodynamic therapy delivered by nano-graphene oxide. *ACS Nano* 5: 7000-7009.
20. Kim JY, Choi W, Kim M, Tae G (2013) Tumor-targeting nanogel that can function independently for both photodynamic and photothermal therapy and its synergy from the procedure of PDT followed by PTT. *Journal of Controlled Release* 171: 113-121. [Crossref]
21. Foster TH, Murant RS, Bryant RG, Knox RS, Gibson SL, et al, (1991) Oxygen consumption and diffusion effects in photodynamic therapy. *Radiat Res* 126: 296-303. [Crossref]
22. Hu XH, Feng Y, Lu JQ, Allison RR, Cuenca RE, et al. (2005) Modeling of a Type II photofrin-mediated photodynamic therapy process in a heterogeneous tissue thantom. *Photochem Photobiol 81*: 1460-1468. [Crossref]
23. Wang KKH, Finlay JC, Busch TM, Hahn SM, Zhu TC, et al. (2010) Explicit dosimetry for photodynamic therapy: macroscopic singlet oxygen modeling. *Journal of Biophotonics* 3: 304-318. [Crossref]
24. Zhu TC, Finlay JC, Zhou X, Li J (2007) Macroscopic modeling of the singlet oxygen production during PDT. *Proc SPIE Int Soc Opt Eng* 6427: 6427O81-6427O812. [Crossref]
25. Zhu TC, Kim MM, Ong YH, Penjweini R, Dimofte A, et al. (2017) A summary of light dose distribution using an IR navigation system for Photofrin-mediated pleural PDT. *Proc SPIE Int Soc Opt Eng* 10047. [Crossref]
26. Lin JT, Cheng DC (2017) Modeling the efficacy profiles of UV-light activated corneal collagen crosslinking. *PloS One* 12: e0175002. [Crossref]
27. Lin JT (2017) Photochemical kinetic modeling for oxygen-enhanced UV-light-activated corneal collagen crosslinking. *Ophthalmology Research* 7: 1-8.
28. Mohammadi Z, Sazgarnia A, Rajabi O, Soudmand S, Esmaily H, et al. (2013) An in vitro study on the photosensitivity of 5-aminolevulinic acid conjugated gold nanoparticles. *Photodiagnosis Photodyn Ther* 10: 382-388. [Crossref]
29. Choi SS, Lee HK, Chae HS (2014) Synergistic in vitro photodynamic antimicrobial activity of methylene blue and chitosan against Helicobacter pylori 26695. *Photodiagnosis Photodyn Ther* 11: 526-532. [Crossref]
30. Zhang J, Jiang C, Longo JPF, Azevedo RB, Zhang H, et al. (2017) An updated overview on the development of new photosensitizers for anticancer photodynamic therapy. *Acta Pharmaceutica Sinica B*.
31. Vijayaraghavan P, Liu CH, Vankayala R, Chiang CS, Hwang KC (2014) Designing multi-branched gold nanoechinus for NIR light activated dual modal photodynamic and photothermal therapy in the second biological window. *Adv Mater* 26: 6689-6695. [Crossref]
32. Zeng C, Shang W, Liang X, Liang X, Chen Q, et al. (2016) Cancer diagnosis and imaging-guided photothermal therapy using a dual-modality nanoparticle. *ACS Appl Mater Interfaces* 8: 29232-29241. [Crossref]
33. Song X, Chen Q, Liu Z (2014) Recent advances in the development of organic photothermal nano-agents. *Nano Res* 8: 340-354.
34. Cai Y, Tang Q, Wu X, Si W, Zhang Q, et al. (2016) Bromo-substituted diketopyrrolopyrrole derivative with specific targeting and high efficiency for photodynamic therapy. *ACS Appl Mater Interfaces* 8: 10737-10742.
35. Shi H, Sun W, Liu C, Gu G, Ma B, et al. (2016) Tumor-targeting, enzyme-activated nanoparticles for simultaneous cancer diagnosis and photodynamic therapy. *J Mater Chem B* 4: 113-120.
36. Wang J, Li Y, Deng L, Wei N, Weng Y, et al. (2017) High-Performance Photothermal Conversion of Narrow-Bandgap Ti_2O_3 Nanoparticles. *Adv Mater* 29: 1603730-1603735.
37. Wang S, Chen Y, Li X, Gao W, Zhang L, et al. (2015) Injectable 2D MoS2-integrated drug delivering implant for highly efficient NIR-triggered synergistic tumor hyperthermia. *Adv Mater* 27: 7117-7122. [Crossref]
38. Guo M, Xiang HJ, Wang Y, Zhang QL, An L, et al. (2017) Ruthenium nitrosyl functionalized graphene quantum dots as an efficient nanoplatform for NIR-light-controlled and mitochondria-targeted delivery of nitric oxide combined with photothermal therapy. *Chem Commun* 53: 3253-3256.
39. Yang X (2018) Nano-Black Phosphorus for Combined Cancer Phototherapy: Recent Advances and Prospects. *Nanotechnology*.